Annual Report **December, 2009**

Physical Limits on Ground Motion From Dynamic Rupture Models with Off-Fault Damage, and Application to Yucca Mountain

Benchun Duan (Texas A&M University) and Steven M. Day (SDSU)

Summary of Main Results/Conclusions

Dynamic rupture models of earthquakes can contribute to the study of physical limits on ground motion at the Yucca Mountain site. Finite strength of the rocks through which seismic waves from earthquake sources propagate is a major factor affecting ground motion at a site. During the past several years, we implemented Mohr-Coulomb plastic yielding into our finite element dynamic code EQdyna and applied EQdyna to the ExGM project. We have completed a study of dynamics of non-planar faults with off-fault plastic yielding (Duan and Day, 2008) and a study of sensitivity of ground motion at Yucca Mountain to uncertainties in fault geometry and fault zone structure (Duan and Day, 2009). The physical model in these calculations is nonlinear in its formulation of both fault friction and off-fault material response, posing significant challenges to numerical solution methods. Therefore, our first step was to verify the computational methodology and we take several measures to do so. First, we compared Andrews' (2005) solution to an elastoplastic rupture problem of this class with our own solution in Duan and Day (2008). We obtain very precise agreement with Andrews' (2005) independent finite difference solution. Second, we compare our finite element solutions at two different element sizes in Duan and Day (2009), again finding very close agreement. Third, we revisit several of the solution of Andrews et al. (2007) in Duan and Day (2009). We are using somewhat different elastoplastic and prestress models than used in Andrews et al. (2007), yet for models that yield similar surface fault slip, we find similar ground motion time histories at the site, indicating that key solution features are robust with respect to minor model variations.

In Duan and Day (2008), we examined how inelastic strain concentrates near a fault kink and the manner in which plastic yielding at the kink then affects both dynamic rupture and seismic radiation. We found that extensive inelastic deformation concentrates near a restraining bend, particularly on the side of the fault associated with rupture-front extensional strains. The extensive inelastic deformation reduces high-frequency radiation from the kink and the reduction is significant above several Hz.

In Duan and Day (2009), we explore the sensitivity of extreme ground motion estimates at Yucca Mountain (the site) to uncertainties in fault geometry, off-fault rock strength, fault zone structure, and undrained poroelastic response of the fluid pressure. The model and calculations of Andrews et al. (2007) form the starting point for the study. For the extreme scenario of nearly complete stress drop on the Solitario Canyon fault, peak ground velocity (PGV) at the site is sensitive to deep fault geometry and cohesive strength of shallow geologic units, while it is relatively insensitive to fault zone structure and pore pressure response. Taking previous estimates of Andrews et al. (2007) as a benchmark, a 10° reduction in dip (from 60° to 50°) of the Solitario

Canyon fault at depth, combined with doubled cohesion of shallow units, can increase both horizontal and vertical PGVs by over 1 m/s, to values exceeding 5 m/s. In a lower stress-drop scenario, PGV is most sensitive to fault geometry at depth, is only modestly affected by fault zone structure, and is insensitive to cohesion of shallow units and pore pressure response. Curves in Key-Figure 1 represent the envelopes of PGV estimates with off-fault yielding. The solid curve corresponds to calculations with cohesion values of Andrews et al. (2007). It shows a bounding PGV of about 4.78 m/s for near-total stress drop events (~15m slip), and about 3.48 m/s for the events with reduced stress drop (~5m slip). The former are supershear rupture-velocity events (which here tend to maximize vertical PGV), while the latter set includes sub-Rayleigh rupture-velocity events (which tends to maximize horizontal PGV). The dashed curve corresponds to calculations with the doubled cohesion values for shallow units. In this case, the PGV bound for near-total stress drop events increases with surface slip (though with a slope much reduced relative to corresponding elastic calculations). Corresponding results for spectral acceleration are shown in Key-Figure 2. Effects of rock strength on spectral acceleration are significant only at short periods (i.e., less than 3 s). Further work should concentrate on examining sensitivity of this bound to the material strength parameters, and, to the extent possible, on obtaining better constraints on their actual values.

Duan also worked on modeling of dynamic rupture along a bimaterial interface with off-fault yielding (Duan, 2008). He found that off-fault damage is highly asymmetric between the two sides of a bimaterial interface, while ruptures in his models propagate bilaterally. Thus, the damage asymmetry observed in some field studies of fault zones could be a consequence of bimaterial effects, but it is not necessarily an indicator for unilateral ruptures, as has sometimes been proposed.

Recommendations for Future Work

1. Additional 2D simulations to examine sensitivity to the material strength parameters.

2. Better constraints on material strength. Mohr-Coulomb strength parameters in Andrews et al. (2007) and Duan and Day (2009) are only generic values correlated with rock types and elastic properties. Better quantitative constraints on these parameters from laboratory tests could improve simulation-based estimates of ground motion extremes.

3. It would also be useful to conduct additional elastoplastic simulations at different stress-drop levels to further elucidate the relationship between extreme PGV and surface fault slip.

4. 3D elastoplastic simulations, with 3D geological structure and fault geometry of the Yucca Mountain region, could place more accurate physical limits on ground motion at the site. This effort would require more computing resources than we have exploited to date.

5. More realistic nonlinear material models--including effects such as irreversible compaction (which Andrews has already begun exploring) and damage rheology (accounting for reduction in elastic moduli during earthquake rupture)--may provide better-refined estimates of the ground motion extremes.

Key Figures of Important Results with Captions

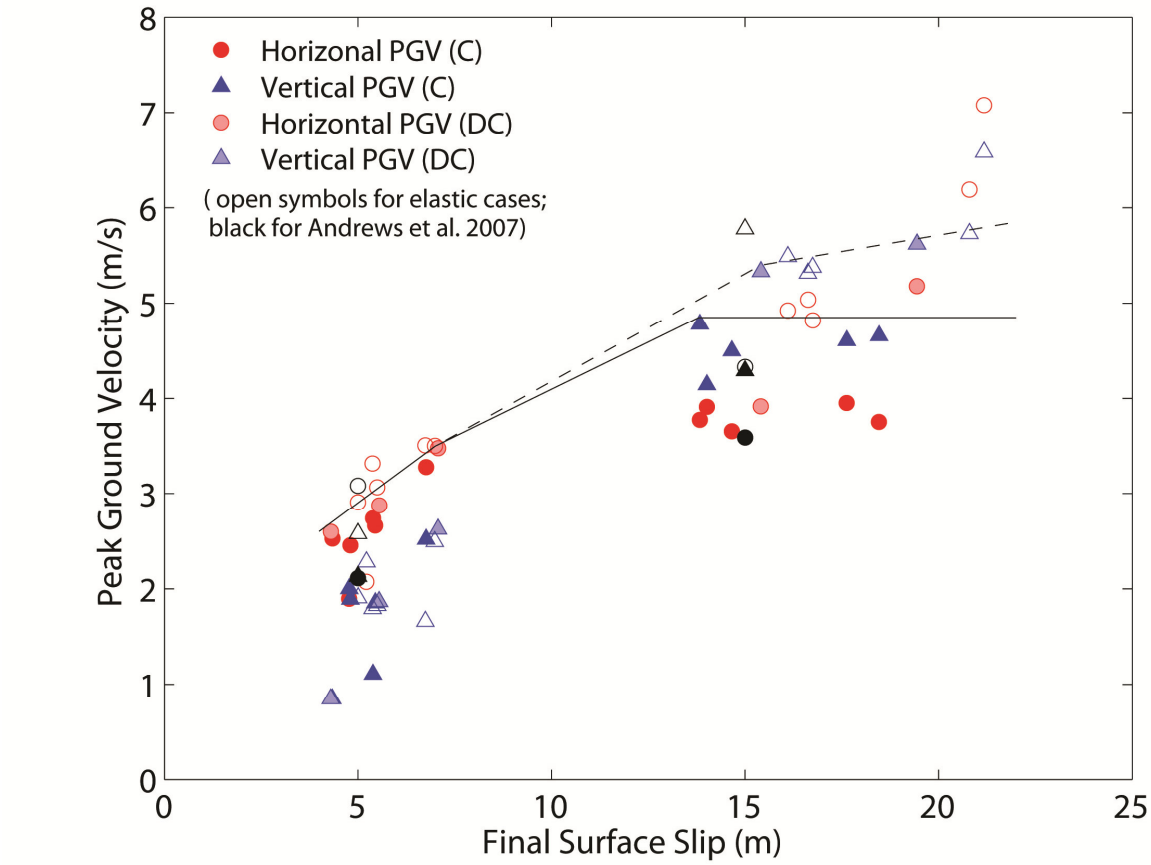

Key-Figure 1. Peak ground velocity (PGV) at the site as a function of surface fault slip from 2D dynamic rupture models of scenario earthquakes on the Solitario Canyon fault. Color symbols are PGV estimates from our simulations, with different shading representing different material strength. Heavy shading (C) denotes PGV estimates with Mohr-Coulomb strength parameter values (cohesion and internal friction angle) of Andrews et al. (2007). Light shading (DC) represents PGV estimates with doubled cohesion values of Andrews et al. (2007) for the shallow geologic units. Open symbols denote results with off-fault elastic response. Black symbols are results from Andrews et al. (2007). Solid and dashed curves are envelopes of PGV estimates with off-fault yielding, corresponding to C and DC calculations, respectively. (From Duan and Day, 2009).

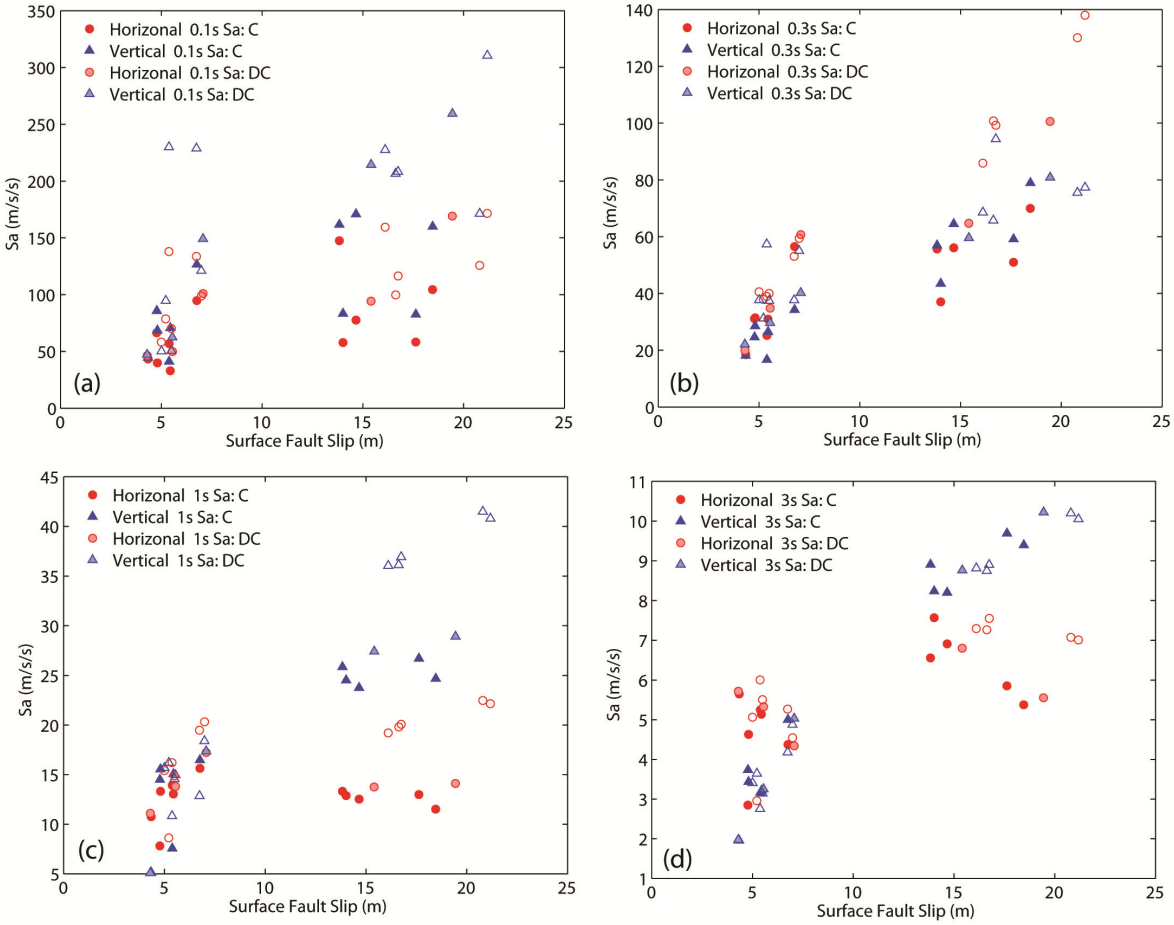

Key-Figure 2. Response spectra (5% damping) from the same calculations included in the previous figure at periods of (a) 0.1 second, (b) 0.3 second, (c) 1.0 second, and (d) 3.0 second. Solid symbols again represent cases with Mohr-Coulomb strength limits, with different shading denoting different cohesion values used in calculations. Open symbols represent cases with off-fault elastic response. The reduction due to yielding is significant only at short periods (i.e., less than 3 second). (from Duan and Day, 2009).

(A)

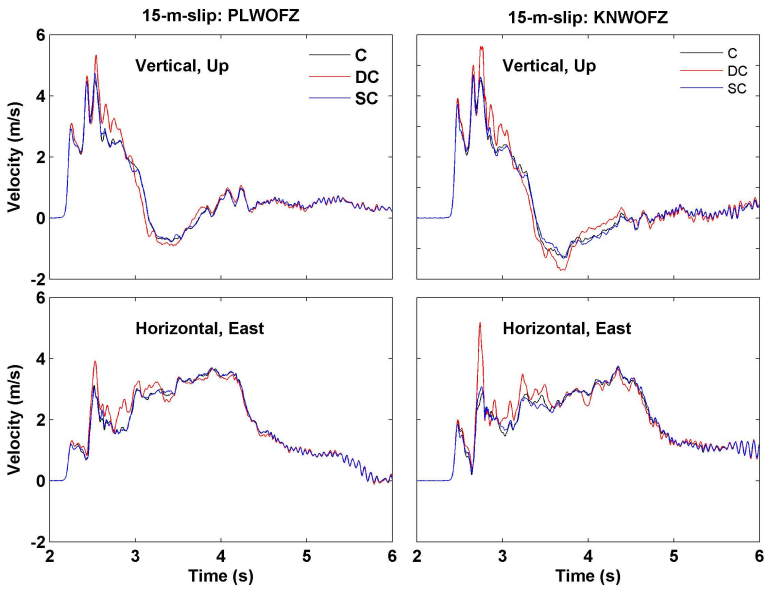

(B)

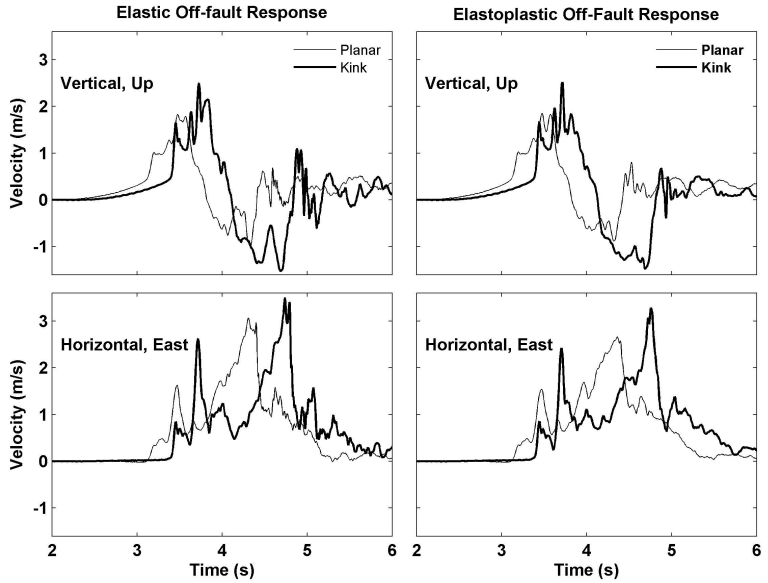

Key-Figure 3. Effects of fault geometry and material strength on ground motion at the site. (A) A shallower dip of the Solitario Canyon fault at depth and doubled cohesion values at shallow depth (red on right panel, DC) results in considerably higher peak ground velocities at the site, compared with the reference case (black on left panel, C) in the nearly complete stress drop scenario. (B) Effects of a shallower dip (Kink) of the Solitario Canyon fault at depth on ground motion with elastic (left panel) or elastoplastic (right panel) off-fault response, compared with the reference (Planar).

Publications From Work Funded Under the ExGM Project

1. Duan, B., and S. M. Day (2009), Sensitivity study of physical limits on ground motion at Yucca Mountain, *Bull. Seismo. Soc. Am.*, submitted (on December 2, 2009).

2. Duan, B., and S. M. Day (2008), Inelastic strain distribution and seismic radiation from rupture of a fault kink, *J. Geophys. Res.*, 113, B12311, doi:10.1029/2008JB005847.

3. Duan, B. (2008), Asymmetric off-fault damage generated by bilateral rupture along a bimaterial interface, *Geophys. Res. Lett.*, 35, L14306, doi:10.1029/2008GL034797.

4. Harris, R.A., M. Barall, R. Archuleta, B. Aagaard, J.-P. Ampuero, H. Bhat, V. Cruz-Atienza, L. Dalguer, P. Dawson, S. Day, B. Duan, E. Dunham, G. Ely, Y. Kaneko, Y. Kase, N. Lapusta, Y. Liu, S. Ma, D. Oglesby, K. Olsen, A. Pitarka, S. Song, and E. Templeton (2009), The SCEC/USGS Dynamic Earthquake Rupture Code Verification Exercise, *Seismological Research Letters*, vol. 80, no. 1, pages 119-126, doi:10.1785/gssrl.80.1.119.

Technical Report

The finite strength of the rocks through which seismic waves from an earthquake source propagate places limits on how large ground motion can be. With support from the ExGM project, we first incorporated Mohr-Coulomb plastic yielding into our finite element dynamic code EQdyna (Duan and Oglesby, 2006, 2007). The Mohr-Coulomb criterion is given by $\tau \le c - \sigma_n \tan\phi$, where τ and σ_n are shear and normal (positive in tension) stresses in any orientation at a point, and c and ϕ are cohesion and the internal frictional angle, respectively. Then we conducted a series of studies of the elastoplastic dynamics of rupture on non-planar faults. These studies examine inelastic strain distribution near a fault kink and how inelastic strain affects rupture dynamics and seismic radiation from the kink. We find that extensive inelastic deformation concentrates near a restraining bend, particularly on the side of the fault associated with rupture-front extensional strains, the deformation taking the form of a few distinct lobes and shear bands (Figure 1). The extensive inelastic deformation can reduce high-frequency radiation from the kink and the reduction is significant above several Hz (Figure 2). The calculated plastic strain distribution around the kink and the radiated pulse from the kink are nearly grid independent over the range of element size for which computations are feasible (Figures 1 and 2). We also find that plastic strain can sometimes localize spontaneously during rupture along a planar fault. However, in this case, the details of the shear banding change with numerical element size, indicating that the final plastic strain distribution is influenced by interactions occurring at the shortest numerically resolvable scales (Figure 3). This result illustrates one of the additional computational challenges introduced when inelastic off-fault deformation is included in rupture models. This work has been published (Duan and Day, 2008) with the SCEC contribution number of 1198.

During the past two years, we worked extensively on 2D dynamic models of the Solitario Canyon fault to address physical limits to extreme ground motion at Yucca Mountain. Our models (Figure 4) take the work of Andrews et al. (2007) as a point of departure. They include geological structure, including tilted layers being offset by normal faults and topography, along the profile that is across the fault and the site under investigation. We first revisit several of solutions of Andrews et al. (2007) (referred to AN07, hereafter). Figure 5 shows results from scenario earthquakes with surface fault slip of ~ 5 m. These results can be directly compared with Figures 21 and 22 of AN07. We are using somewhat different elastoplastic and prestress models than used in AN07, yet for models that yield similar surface slip, we find similar ground motion time histories at the site, indicating that key solution features are robust with respect to minor model variations.

Then we explore effects of several factors in the source region on ground motion extremes at the site. These factors include time-dependent pore pressure, a possible shallower dip of the fault at depths, and the presence of a possible low-velocity fault damage zone. In each case, we perform two calculations, one with elastic off-fault response and the other with elastoplastic off-fault response.

Time-dependent pore pressure has minor effect on ground motion at the site, relative to models with constant pore pressure (Figure 6). The effect is more visible in elastoplastic calculations than in elastic calculations. This is because pore pressure affects off-fault material strength, thus the degree of plastic yielding (Figure 7).

A seismic reflection survey (Brocher et al., 1998) shows that the Solitario Canyon fault has a shallower dip at depth compared with that near the surface. Given the same seismogenic depth, the shallower dip at depths (50° versus 60°) results in a longer rupture length. When we also double the cohesion values of Andrews et al. (2007) for shallow geologic units, this shallower dip at depth results in a significantly larger peak slip velocities at the site (see Key-Figure 3a).

We also examine effects of a possible low-velocity damage fault zone (100 m wide, symmetric about the fault). We find that the low-velocity fault zone has little effect on ground motion at the site in the nearly complete stress drop calculations. But in a lower stress drop case, the low-velocity results in a much stronger second peak of vertical velocity if off-fault response is elastic. With elastoplastic off-fault response, the low-velocity fault zone significantly reduces the vertical peak ground motion (PGV) (Figure 7).

We summary peak ground velocity (PGV) as a function of surface fault slip from all simulations we have performed. This results is shown in Key-Figure 1. Similar results for spectral acceleration are shown in Key-Figure 2. This part of our research was submitted to the *Bulletin of Seismological Society of America* (Duan and Day, 2009).

References

Andrews, D. J., T. C. Hanks, and J. W. Whitney (2007), Physical limits on ground motion at Yucca Mountain, *Bull. Seismol. Soc, Am.*, 97, 1771-1792, doi:10.1785/0120070014.

Brocher, T. M., W. C. Hunter, and V. E. Langenheim (1998), Implications of seismic reflection and potential field geophysical data on the structural framework of the Yucca Mountain-Crater Flat region, *GSA Bulletin*, v. 110, no. 8, 947-971.

Duan, B., and S. M. Day (2008), Inelastic strain distribution and seismic radiation from rupture of a fault kink, *J. Geophys. Res.*, 113, B12311, doi:10.1029/2008JB005847.

Duan, B., and D. D. Oglesby (2007), Nonuniform prestress from prior earthquakes and the effect on dynamics of branched fault systems, *J. Geophys. Res*., 112, B05308, doi:10.1029/2006JB004443.

Duan, B., and D. D. Oglesby (2006), Heterogeneous fault stresses from previous earthquakes and the effect on dynamics of parallel strike-slip faults, *J. Geophys. Res*., 111, B05309, doi:10.1029/2005JB004138.

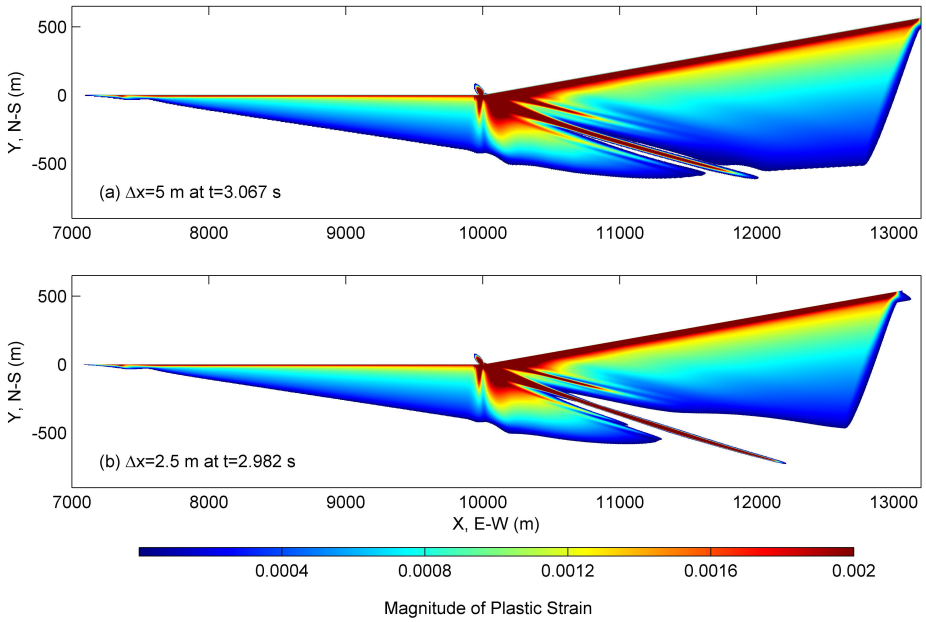

Figure 1. Distribution of off-fault plastic strain magnitude due to rupture on a fault with a kink (at x = 10 km, y = 0 km). Plastic strain localizes into bands and lobes near the kink, and the solution of the localization is apparently convergent when the element size is reduced. (From Duan and Day, 2008).

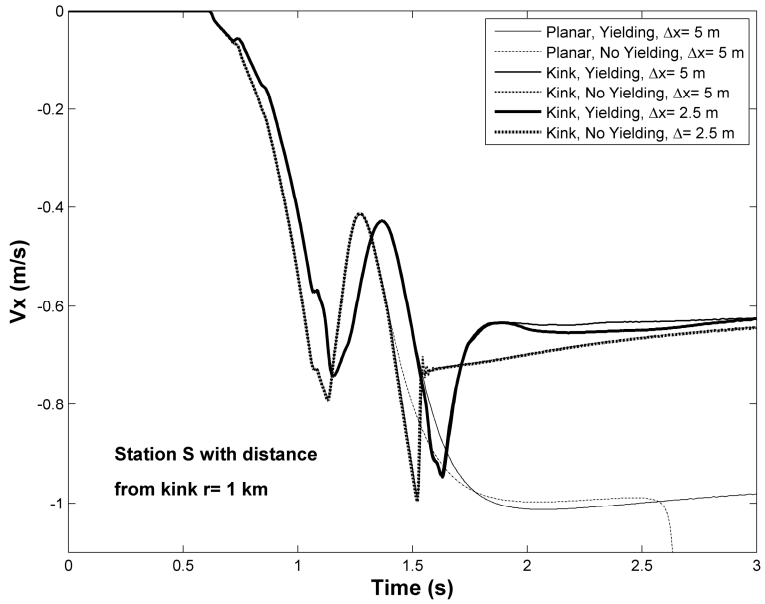

Figure 2. Particle velocity time histories from six simulations. Velocity jumps beyond 1.5 s from the kink fault model are caused by seismic radiation from the kink. Plastic yielding near the kink reduces high-frequency radiation from the kink (indicated by a larger rise time). (After Duan and Day, 2008).

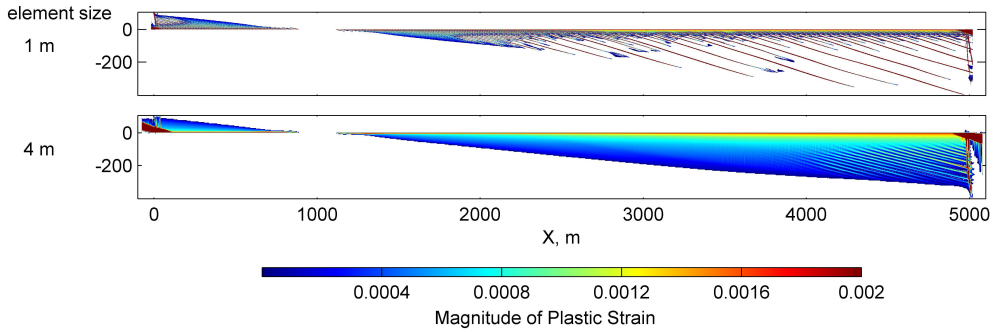

Figure 3. The distribution of plastic strain magnitude in a planar fault model with two different element sizes. Features of plastic strain localization keep changing with the element size, imposing a challenging in numerically simulating the localization. (From Duan and Day, 2008).

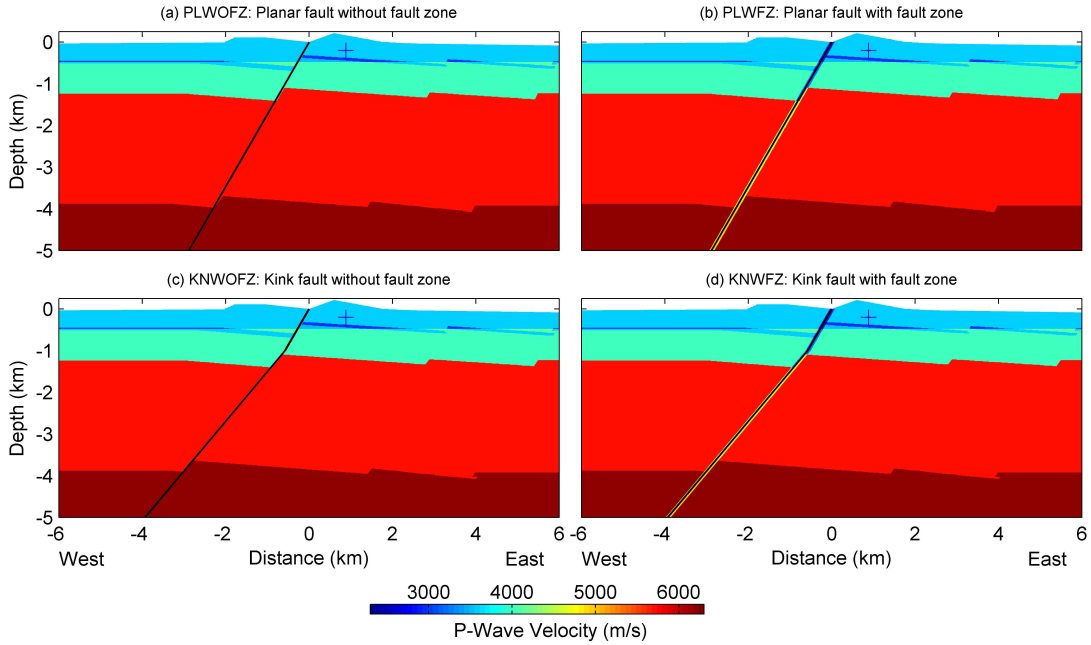

Figure 4. Different fault models to examine effects of fault geometry and fault zone structure of the Solitario Canyon fault (black line) on ground motion at the site (plus sign). (a) PLWOFZ and (b) PLWFZ are planar fault models, while (c) KNWOFZ and (d) KNWFZ are kinked fault models with a change in dip from 60° to 50° at depth of 1 km. Fault zone is absent in (a) and (c), while a 100 m wide fault zone bisected by the fault is present in (b) and (d). In the fault zone, seismic wave velocities (both P and S) of rock are reduced 20% relative to those of lateral surrounding wall rock. (From Duan and Day, 2009).

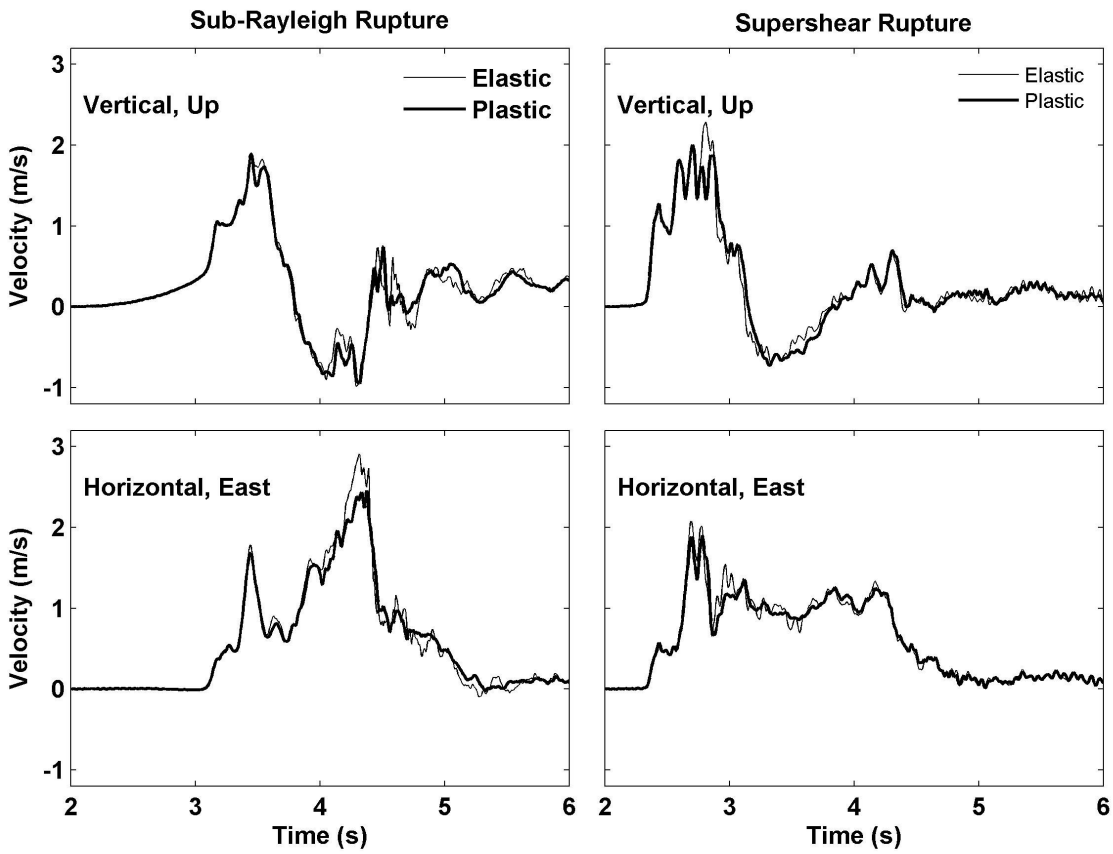

Figure 5. Comparison of ground velocity at the site between sub-Rayleigh rupture (left) and supershear rupture (right), between elastic (light curve) and elastoplastic (heavy curve) off-fault responses in the case with surface slip of ~ 5 m. These time histories can be compared with those in Figures 21 and 22 of AN07. (From Duan and Day, 2009).

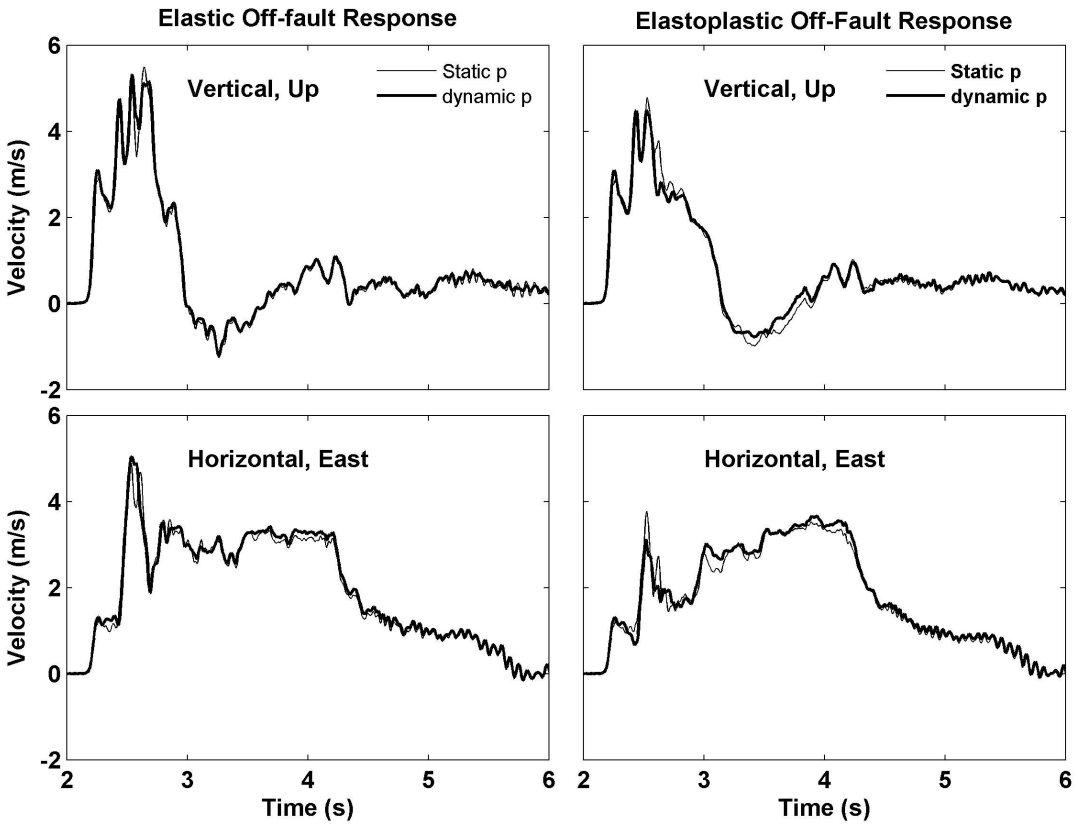

Figure 6. Effects of time-dependent pore fluid pressure (dynamic p) on ground motion at the site in the case of ~ 15 m surface slip with supershear rupture. Compared with ground motion with a constant pressure (static p), time-dependent pore pressure has minor effect on ground motion at the site. The effect is more visible in elastoplastic calculations than in elastic calculations. (From Duan and Day, 2009).

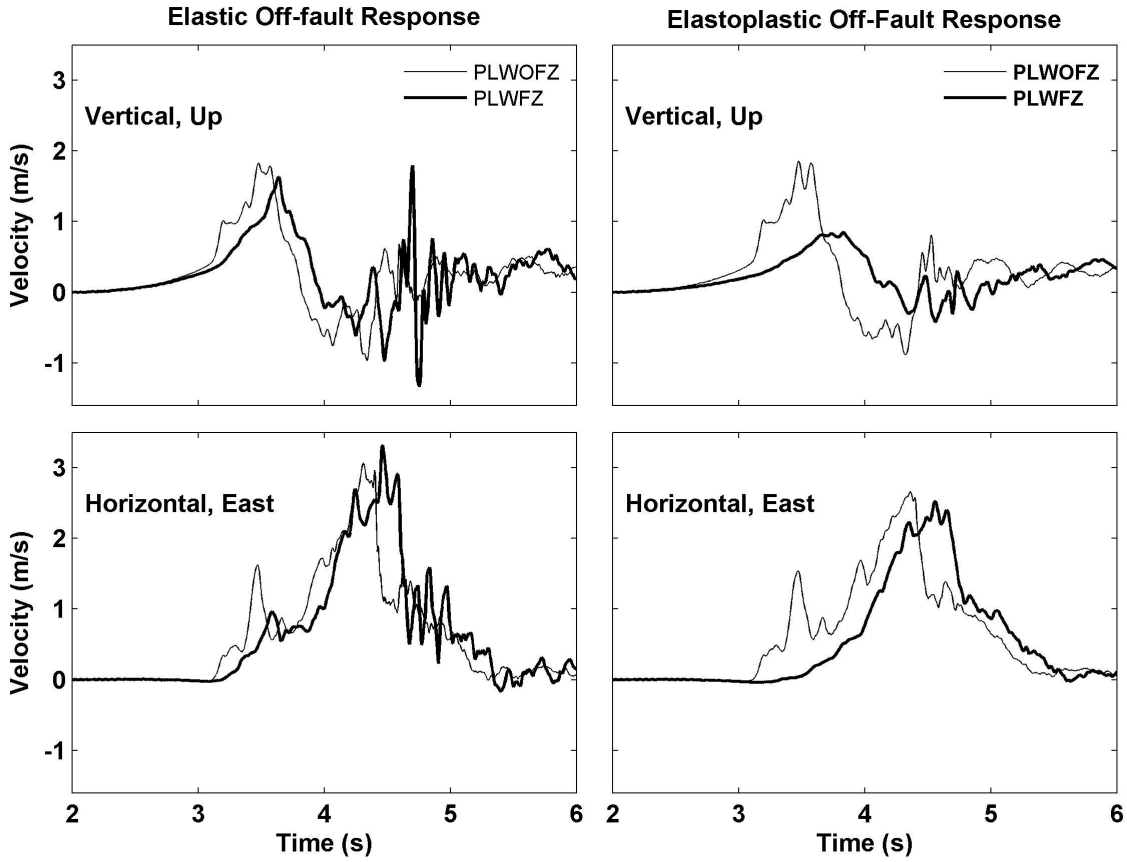

Figure 7. Effects of a 100-m wide low-velocity fault zone (PLWFZ, with a reduction in seismic wave velocity of 20% relative to wall rocks) surrounding the Solitario Canyon fault on ground motion at the site, in dynamic calculations with off-fault elastic response (left panel) and off-fault elastoplastic response (right panel).